Dynamics of Thermal Electron Emission from Highly Excited C60

Cite as:
Johansson, J.O., Henderson, G.G., Campbell, E.E.B. (2014). Dynamics of Thermal Electron Emission from Highly Excited C_{60}. J. Phys. Chem. A., 118(37), 8067–8073.

Manuscript received: 14/08/2013; Accepted: 29/10/2013; Article published: 31/10/2013

Dynamics of Thermal Electron Emission from Highly Excited C_{60}

J. Olof Johansson, Gordon G. Henderson and Eleanor E.B. Campbell[*]

EaStCHEM, School of Chemistry, University of Edinburgh, Edinburgh EH9 3JJ, UK

KEYWORDS Fullerenes, photoelectron spectroscopy, photoelectron angular distributions, femtosecond spectroscopy, atomic and molecular clusters, photon interaction with molecules

ABSTRACT Gas-phase fullerenes emit thermal electrons after femtosecond laser excitation in the wavelength range 400 – 800 nm. We have used angular-resolved photoelectron spectroscopy (PES) to study the influence of the laser's electric field on the dynamics of the thermally emitted electrons. The laser field introduces an asymmetry in the thermal electron distributions with respect to the laser polarization direction, which was confirmed by carrying out experiments at different wavelengths. A simple model could reproduce the trends in measured apparent

temperatures in the PES. The asymmetry effect was exploited in a pump-probe experiment to estimate the timescale for thermal electron emission. It was found that, when using 400 nm, 120 fs laser pulses of 2 TW cm^{-2} intensity, thermal electrons are emitted up to *ca*. 300 fs after the peak of the laser pulse. The pump-probe scheme should be applicable to a wider range of complex molecules and clusters showing thermal electron emission on a fs timescale.

INTRODUCTION

The properties of photoexcited carbon nanoparticles and large organic molecules are of interest for the development of organic photonics, electronics and photovoltaic devices. Fullerenes can be considered as nanoscale carbon clusters and are ideal model systems to achieve a deeper understanding of these systems because their high symmetry and simple chemical composition simplifies theoretical modeling.[1] An additional advantage of using fullerenes is that it is relatively straightforward to produce a beam of neutral, mass dispersed molecules in the gas-phase, which is ideal for studying intramolecular decay processes since there is no coupling to any surrounding surfaces or solvents.

Femtosecond laser pulse excitation of C_{60} using photon energies lower than the ionization energy results in rapid redistribution of the excitation energy among the valence electrons before the onset of significant coupling to vibrational degrees of freedom.[2–5] Due to the low photoionization rate of the excited valence states (on the order of 10^{10} s^{-1}) during the *ca*. 100 fs laser pulse of moderate intensity (10^{11} – 10^{13} Wcm^{-2}), these states will not directly ionize.[6] Instead, the molecules continue to absorb more energy from the pulse which eventually leads to the emission of thermal electrons. These thermal electrons show an exponential kinetic energy distribution in photoelectron spectra (PES), $I(\varepsilon) \propto \exp(-\varepsilon/k_B T_a)$, with ε being the electron kinetic energy and T_a the apparent electron temperature. The latter can give insights into the

thermodynamical properties of the valence electrons and the coupling to vibrational degrees of freedom. The thermal electrons of interest here should not be confused with thermionic electron emission that is observed from fullerenes[7] and some other cluster species after coupling to the vibrational degrees of freedom has occurred.[8] Thermionic electron emission is seen to occur after excitation with ps or ns laser pulses and takes place on a much longer, microsecond timescale. Other species such as larger fullerenes,[4,9] endohedral fullerenes,[9,10] sodium clusters,[11,12] and polycyclic aromatic hydrocarbons (PAHs)[13] have all been reported to show thermal photoelectron spectra following excitation with fs laser pulses.

In fullerene fs PES, a series of clear peaks are also observed superimposed on the thermal background. These peaks are attributed to single-photon ionization of diffuse Rydberg-like states, which have much higher photoionization rates (on the order of 10^{14} s^{-1}) than the more localized valence states and are therefore promptly photoionized during the fs laser pulse.[6,14] This paper, however, focuses on the electrons with a thermal kinetic energy distribution.

Based on relatively simple modeling of a transient thermal emission mechanism, occurring before the excitation energy is coupled to vibrational modes, the majority of the thermal electrons are expected to be emitted during the timescale of the excitation laser pulse.[3] However, since the emission is thermal, the emission time is expected to be uncorrelated with the phase of the laser electric field. This was shown in Ref. [5] to lead to an asymmetry in the electron kinetic energy distributions with respect to the laser polarization direction since thermal electrons emitted at the peak of the vector potential (zero electric field) will gain an additional momentum kick along the polarization direction. This is a well-known phenomenon, explained by classical electrodynamics, and is often used in attoscience for pulse duration measurements.[15] In the present study, we have verified this hypothesis with measurements using different laser

wavelengths and have also used the asymmetry effect in a pump-probe scheme to estimate the timescale for thermal electron emission.

The paper is organized as follows. In the first part of the paper, the experimental setup and the simple model describing the temporal evolution of the internal energy of the fullerene's electronic system are described. In the second part of the paper, the measured asymmetry for a number of different laser wavelengths is presented, and is seen to support the proposed interpretation. The results of the simple model are then compared to the experimental results and reasonable agreement is found. In the final part of the paper, the field interaction with the emitted electrons is used to estimate the timescale of thermal electron emission from highly electronically excited fullerenes using a pump-probe scheme.

METHODS

EXPERIMENTAL SETUP

The experimental setup is shown in **Figure 1** a). An effusive molecular beam was obtained by heating purified C_{60} powder (99.95% purity, SES Research) in an oven to 500 °C (see **Figure 1** b). The oven was situated in a vacuum chamber below a larger vacuum chamber, where the molecules were ionized, and the two chambers were connected through a 4 mm diameter orifice. Ion optics, electron and ion detectors were mounted in the larger chamber (**Figure 1** a). Pressures in both chambers were $\leq 10^{-8}$ mbar.

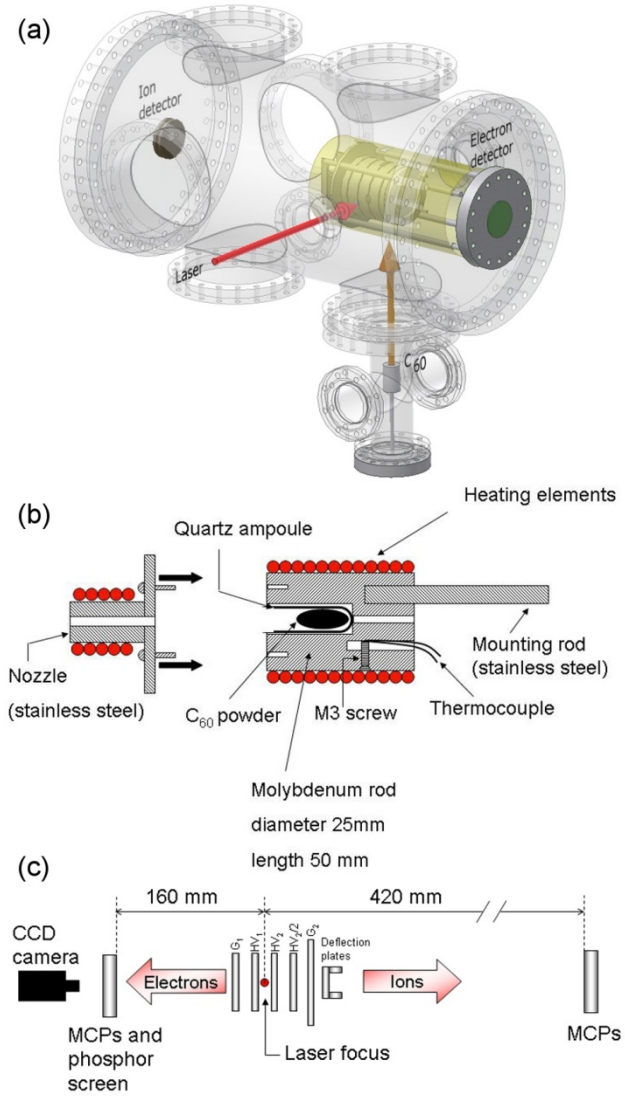

Figure 1. (a) Sketch of the experimental setup. Fullerenes are sublimed into the gas-phase in the lower vacuum chamber. (b) Sketch of the fullerene oven (situated in the lower chamber in (a)). C_{60} powder is placed in the quartz ampoule and sublimed at *ca*. 500 °C to produce an effusive molecular beam. (c) Ion optics configuration. Electrons are extracted to the position-sensitive detector using an electrode configuration allowing for velocity-map imaging.[16] Ions are extracted to a time-of-flight mass spectrometer. Electrodes HV_2, $HV_2/2$ and G_2 have a 90 % transmitting metallic mesh installed to create a flat extraction field, in contrast to the open VMI electrodes.

The 800 nm, 110 fs output of a Ti:Sapph regenerative amplifier was used for the experiments. The second harmonic, generated in a BBO crystal was also used. The regenerative amplifier pumped a commercial non-collinear parametric amplifier (NOPA) producing pulses with tuneable wavelength in the range 490 – 1100 nm. A half-wave plate and a Glan-laser polarizer were used to control the laser power and polarization direction. The pulse duration was measured using a home-built second-order autocorrelator consisting of a BBO doubling crystal and the pulse duration of the NOPA was determined to be in the range 50 – 90 fs after passing through the waveplate, polarizer and a vacuum viewport (consisting of 2.5 mm of Kodial glass). The laser beam was focused (f = 30 cm) into the vacuum chamber and the intensity was estimated by using the properties of Gaussian beams when focused in combination with the measured pulse duration and energy. Multiphoton ionization via Freeman-type resonances in Xe was also used to calibrate the laser intensity in the laser focus.[17] The agreement between the two methods was better than 15 %.

The laser beam intersected the effusive molecular beam at right angles and the photoproducts were extracted using a similar set of electrodes to those in Ref.[4] The ions were extracted into a linear time-of-flight (TOF) mass spectrometer using a set of electrodes in a Wiley-McLaren configuration with a typical acceleration voltage of 3 kV, as shown in Figure 1 c). The ions were detected using a chevron-style MCP detector and after passing the signal through a preamplifer and an oscilloscope, the ion TOF spectra were recorded on a computer using a LabVIEW program. The electrons were extracted using a set of electrodes allowing for velocity-map imaging onto a combination of MCPs and a phosphor screen. The image on the screen was recorded using a CCD camera and typically 10^6 – 10^7 laser shots were used to produce one VMI image. The images were subsequently inverted using a modified version of POP[18] (including up

to the 10th Legendre polynomial). The inverted VMI images were integrated in 10° angular segments to get the angular resolved PES, which were subsequently analysed by fitting a thermal distribution to each spectrum. Typically, the fitted apparent temperatures along the laser polarization direction were compared to the apparent temperatures fitted perpendicular to the laser polarization direction.

For the pump-probe experiment, 400 nm pulses were used as the pump and the 60 fs, 900 nm output from the NOPA was the probe. The delay between the two beams was controlled using a motorized translation stage. The sum-frequency generation (SFG) signal of the two beams was recorded outside the chamber and gave a FWHM of 140 fs. The two beams were then passed collinearly through the vacuum chamber using a dichroic mirror and after the output vacuum window, a concave metallic mirror (f = 30 cm) focused the two beams back into the vacuum chamber. Xe ion yields were recorded to determine time zero. Once time zero had been established, VMI images were collected as a function of pump-probe delay and subsequently inverted and analyzed to obtain the apparent temperatures along and perpendicular to the laser polarization direction.

COMPUTATIONAL DETAILS

For relatively large molecules, such as C_{60}, the large density of states leads to an efficient energy redistribution through the population of a wide range of vibronic states. It is therefore very demanding to model the dynamics of highly excited fullerenes using an *ab-initio* method. A simpler approach is to consider the valence electrons as a free-electron gas that is heated by the incoherent absorption of photons from the laser pulse. The energy absorbed by the electrons will eventually couple to the vibrational degrees of freedom of the molecule, quenching the electronic excitation energy.

The calculation of the temporal evolution of the internal energy $E(t)$ of the electronic system of the fullerenes can be used as an input to model the electron emission via a simple first-order decay to obtain emission rate constants, which in turn can be used to calculate experimental observables such as the apparent electron temperature. We follow the procedure used in Refs[4,5,13]. The internal energy is calculated by solving the following differential equation

$$\frac{d(E(t))}{dt} = \sigma_p I(t) - \frac{E(t)}{\tau} \tag{1}$$

where σ_p is a constant, average photon absorption cross-section, $I(t)$ is the laser intensity, assumed to have a Gaussian time dependence, and τ is the time constant for coupling to vibrational degrees of freedom (set to 240 fs based on the work in Ref. [3]). The equation is solved using Matlab's ODE solver. This model assumes that the energy relaxation to vibrational degrees of freedom can be described with a single decay constant τ that is independent of the energy difference between the electronic and vibrational systems. A better description would be provided by a two-temperature model where the coupling constant is dependent on the temperature difference. However, to gain a qualitative understanding of the underlying physics we have kept the model as simple as possible. A simple Arrhenius-type expression is used for the emission rate constant as a function of electron temperature:[19]

$$k(T) = A_0 \exp(-\Phi / k_B T), \tag{2}$$

where $A_0 \approx 2.7 \times 10^{15}$ s^{-1} (value from Ref. [5]), Φ is the ionization potential of C_{60} (7.6 eV) and the electron temperature T is close to the mean of the neutral and ion temperatures. By treating the valence electrons as a free electron gas, it is possible to estimate $T(t)$ from Fermi-Dirac statistics[20]

$$k_B T(t) = \sqrt{4E(t)E_F / \pi^2 N}, \tag{3}$$

where N is the number of valence electrons (240 for C_{60}) and $E_F \approx 20$ eV is the Fermi energy (equivalent to the chemical potential at absolute zero, $E_F = \left(\frac{3\pi^2 N}{V}\right)^{2/3} \frac{\hbar^2}{2m_e}$, with V the volume of the C_{60} shell (and m_e the mass of the electron).

The number of neutral molecules in the beam is *n(t)* and assuming first-order kinetics, the rate of ionization is

$$\frac{dn(t)}{dt} = -k\big(E(t')\big)n(t). \tag{4}$$

Due to the relatively low laser intensities used in this work, multiply charged species were omitted in the calculations. Separating variables and integrating Eq. (4) yields

$$\int_{n_0}^{n} \frac{1}{n} dn = -\int_{-\infty}^{t} k\big(E(t')\big)dt'. \tag{5}$$

This gives the surviving fraction of neutral molecules at time t

$$P(t) = \frac{n(t)}{n_0} = \exp\left[-\int_{-\infty}^{t} k\big(E(t')\big)dt'\right]. \tag{6}$$

The time-dependent electron yield is related to the number of surviving molecules as

$$Y(t) = -\frac{dP(t)}{dt} = k(t) \times \exp\left[-\int_{-\infty}^{t} k\big(E(t')\big)dt'\right]. \tag{7}$$

The photoelectron spectrum (PES) can be well-approximated with an exponential kinetic energy distribution characterised by the apparent electron temperature $T_a \approx T - \Phi/2C_v$, (here, the heat capacity of a 3D Fermi gas has been used $C_v = \pi^2 k_B^2 NT/2E_F$). A detailed discussion on micro-canonical temperatures in finite systems can be found in refs.[19,21]

The instantaneous photoelectron spectrum F_{PES} at $t = t'$ is given by

$$F_{PES}(\varepsilon, t') = \frac{Y(t')}{k_B T_a(t')} \exp\left(-\frac{\varepsilon}{kT_a(t')}\right), \tag{8}$$

where ε is the electron kinetic energy and $k_B T_a$ is included outside the exponent for normalization reasons when integrating over all kinetic energies. By calculating F_{PES} for each time step and each point in the focal volume (taking into account the temporal and spatial variation of the laser intensity using the same laser beam parameters that are used in the experiments), the total PES is calculated. The results show that the total PES obtained in this way can be well approximated with an exponential distribution and apparent temperatures can be fitted and compared to experiments. The values for the pre-exponential factor[5] A_0 and the vibrational coupling time constant[3] τ are taken from previous work and the only fit parameter used here is the average photon absorption cross section σ_{p}.

To calculate the momentum kick from the field, the magnitude of the vector potential along the polarization direction is calculated $A = E_0/\omega \sin(\omega t_0)$, where E_0 is the electric field amplitude, ω is the laser angular frequency and t_0 is the time of electron emission. For each time step, the instantaneous PES (eq. 8) is calculated using the approach outlined above and is converted from a kinetic energy distribution (no information of directionality) into a momentum distribution to distinguish between electrons emitted up or down with respect to the sign of the instantaneous vector potential. The distribution is subsequently shifted by the amount eA (e is the elementary charge) in a direction that is given by the sign of A. The shifted distribution is then converted back into a kinetic energy distribution and used to obtain the total PES. By switching the momentum transfer on and off, we can compare the asymmetry in apparent temperature along and perpendicular to the laser polarization direction.

RESULTS AND DISCUSSION

APPARENT TEMPERATURES

In **Figure 2** (a), a VMI distribution is shown after exciting C_{60} using 120 fs laser pulses of 400 nm wavelength and 1.4 TW cm^{-2} intensity. The 0 – 10 degrees angular-resolved PES (approximately parallel to the laser polarization direction) and the 80 – 90 degrees segment are shown in **Figure 2** (b). Apart from the structure seen mainly in the parallel spectrum, the two apparent temperatures are similar, seen from the similar slopes on the ln-lin plot. For longer wavelengths, the photon absorption cross section is lower, which means that a higher laser intensity is needed to achieve a similar apparent temperature as compared to short-wavelength excitation. When exciting with 800 nm, there is a clear difference in the velocity distribution in **Figure 2** (d) compared to the one obtained after 400 nm excitation (a). The velocity distribution is not isotropic for the longer wavelength and in the angular-resolved PES a significantly higher apparent temperature is measured along the laser polarization direction compared to the perpendicular direction.

For the intensities and wavelengths used in **Figure 2**, the perpendicular apparent temperatures are similar and so are the corresponding mass spectra. The fragmentation pattern in the mass spectrum is indicative of the amount of energy deposited in the molecule by the laser.[22,23] Since the mass spectra and the apparent temperature fitted to the perpendicular PES for the two wavelengths are similar, the energy deposited by the laser pulse can be assumed to be similar and we argue that the perpendicular temperature, in contrast to the parallel temperature, is a useful measure of the absorbed energy. This was also proposed by Huismans *et al*.[24] and is used in the next section to compare apparent temperatures, calculated using the simple model, to experimental results. The asymmetry is also discussed further in the next section.

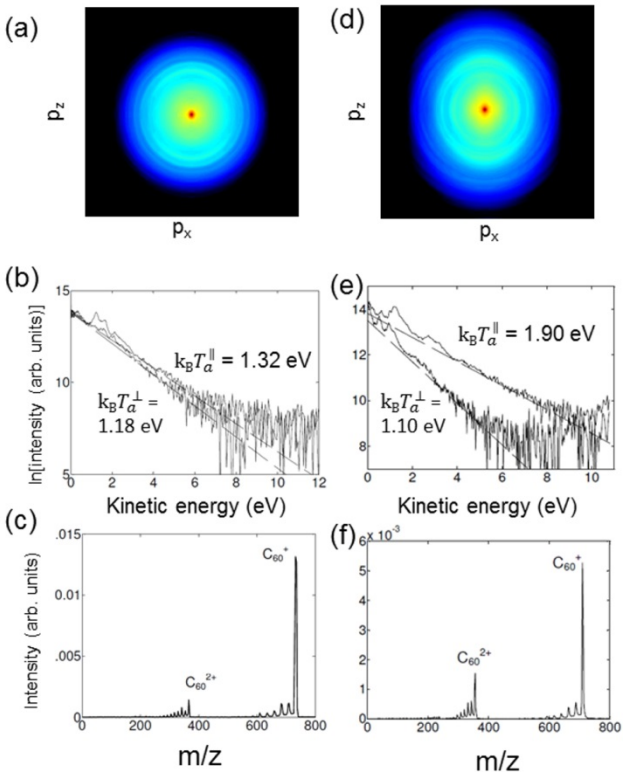

Figure 2. Experimental results obtained using two different wavelengths. In (a), an inverted VMI image (plotted in logarithmic color scale for display purposes) is shown after 400 nm, 1.4 ± 0.2 TW cm^{-2}, 120 fs excitation. A near-isotropic electron distribution is observed (laser polarization direction parallel with the momentum p_z). The angular resolved PES parallel and perpendicular to the laser polarization direction are shown in (b). The corresponding mass spectrum is shown in (c). The right-hand side panels (d – f) were obtained using 800 nm, 182 fs and 6.7 ± 0.2 TW cm^{-2} excitation.

ASYMMETRIC THERMAL ELECTRON EMISSION

In the simple model, the electron gas absorbs energy from the laser field and reaches a high temperature very rapidly. The increased temperature leads to the emission of electrons that, due

to the thermal, statistical nature of the process, is uncorrelated with the phase of the electric field of the laser at the moment of ionization. However, if the electrons are emitted while the laser pulse is still present, the oscillating electric field of the laser can influence the kinetic energy of the emitted thermal electrons, which was recently explained using a model based on classical electrodynamics.[1,5] More generally, an electron born in a time-varying electric field will experience a momentum kick along the polarization direction, proportional to the instantaneous value of the vector potential at the time of birth. When an electron is emitted at the peak of the electric field, as in direct photoionization, the vector potential is zero and the increase in velocity of the electron will be zero after the pulse. If, on the other hand, the electron is born when the electric field is zero, corresponding to a maximum value of the vector potential, the electron gains up to $2U_p$ in kinetic energy. Here U_p is the average kinetic energy of a free electron in a time-varying electric field and is given by $U_p\,(\mathrm{eV}) = 9.34 \times [\lambda\ (\mathrm{nm})]^2 \times I\ (\mathrm{Wcm^{-2}})$ where λ is the wavelength and I the peak intensity of the field. Since thermally emitted electrons are uncorrelated with the phase of the electric field, in contrast to electrons produced by direct photoionization, a fraction of the thermal electrons will be emitted at times when there is a finite vector potential. These electrons will experience a push along the laser polarization direction, causing the experimentally observed asymmetry in the velocity distributions. As can be seen in **Figure 3** a), the difference in apparent temperature along and perpendicular to the laser polarization direction falls approximately between U_p and $2U_\mathrm{p}$ for a range of wavelengths, which supports the proposed mechanism.

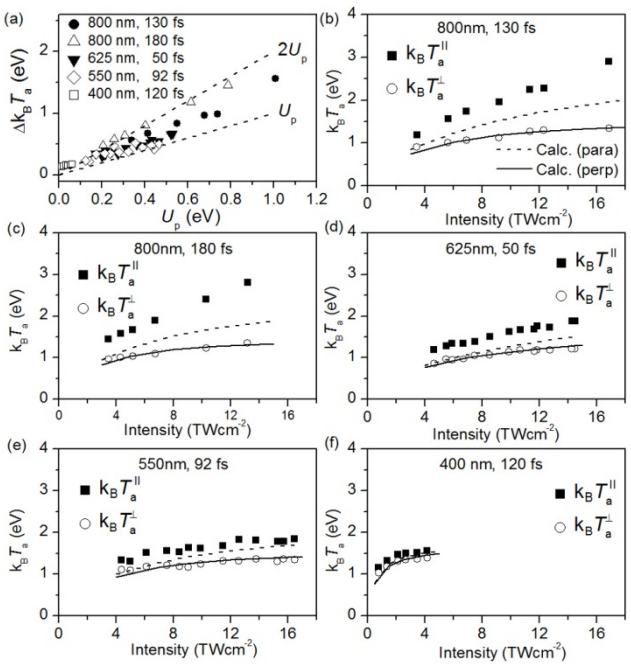

Figure 3. (a) The difference in apparent temperature parallel and perpendicular to the laser polarization direction for a range of wavelengths and pulse durations. The laser intensity for each measurement has been converted to U_p (x-axis). (b) – (f) Experimental and computational results for parallel (squares: experiments; dashed lines: computations) and perpendicular (circles: experiments; solid lines: computations) apparent temperatures. Calculations were obtained using the model described in the Methods section with parameters $A_0 = 2.7\times10^{15}$ s^{-1} and a time constant for vibrational coupling of 240 fs. The average photon absorption cross-sections used for the various wavelengths were (b) $\sigma_p = 0.15$ Å^2, (c) same as (b), (d) $\sigma_p = 0.265$ Å^2, (e) $\sigma_p = 0.23$ Å^2 and (f) $\sigma_p = 1.00$ Å^2.

The degree of asymmetry will depend on when the bulk of the electrons are emitted with respect to the phase and magnitude of the laser field (also taking into account the focal volume). To gain more insights, we have used the model presented in the Methods section using only the photon absorption cross-section as a fit parameter to fit the current data. As can be seen in **Figure 3** (b – f), the calculations can reproduce the intensity dependence of the perpendicular

apparent temperature rather well, despite the simplicity of the model. However, the model consistently gives a lower value for the apparent temperatures along the laser polarization direction. Reasons for this remain unclear but from the model it is clear that the calculated emission times are more sensitive to the choice of parameters than the calculated apparent temperatures. This will influence the asymmetry more than it will influence the perpendicular apparent temperatures. Other effects, not considered in the simple model, might be expected to contribute as well, such as the internal polarization, re-collision effects or smeared-out above-threshold ionization (ATI) peaks. Furthermore, the thermal model could be improved by using a more accurate density of states and calculating the rate constant using detailed balance.[3] All these effects should be considered in more detail and could potentially improve the agreement between the model and the experiments. However, despite the failings of the simple model to quantitatively reproduce the asymmetry, the results presented in **Figure 3** indicate that the proposed mechanism is indeed in good qualitative agreement with trends observed in experimental data.

TIME-RESOLVED THERMAL ELECTRON EMISSION

Controlling the relative phase of an IR field with respect to the birth of a photoelectron and thereby giving the electron a kick along the laser polarization direction is frequently used in attosecond science to measure temporal events, using a technique similar to a streak camera.[15] Since delayed (with respect to the excitation pulse) thermal electron emission has not been measured explicitly for fullerenes excited with fs laser pulses, in contrast to the case for the slower microsecond timescale thermionic electron emission observed when exciting with ns laser pulses,[7,8,25] we have investigated the possibility to use the streaking mechanism to observe

delayed electron emission on a fs time scale. When exciting using 100 – 200 fs pulses it has been estimated that the rate constant from the thermal electron emission model is consistent with electron emission on the 100s of fs timescale.[3]

There have been pump-probe experiments reported on thermal ionization of cationic Na clusters although these experiments monitored the timescale for coupling to vibrational degrees of freedom, and did not explicitly measure any delayed electron emission.[12] Due to the efficient ionization of Rydberg states,[6] it is not trivial to extract relevant information in a C_{60} ion yield pump-probe scheme. Our approach was therefore the following. We used a short-wavelength laser pulse (400 nm, low U_p) to generate near-isotropic thermal electron emission (c.f. **Figure 2** a). Introducing a low-energy IR pulse (900 nm, *ca*. 60 fs) with shorter pulse duration than the first pulse, will give the electrons a relatively large kick, due to the strong wavelength dependence of U_p, along the laser polarization direction without causing any significant extra heating due to the low pulse energy. Ideally, an even longer probe wavelength should be used but a compromise between long wavelength and available NOPA power was made. All electrons emitted during or prior to the IR pulse will follow the IR field, but only those electrons that are born within the temporal envelope and at, or close to, the peaks of the IR pulse's vector potential will get a measurable final kick from the pulse (**Figure 4** a – e). Therefore, by monitoring the asymmetry in apparent temperature parallel and perpendicular to the laser polarization direction as a function of time, it should be possible to measure delayed electron emission on the fs timescale.

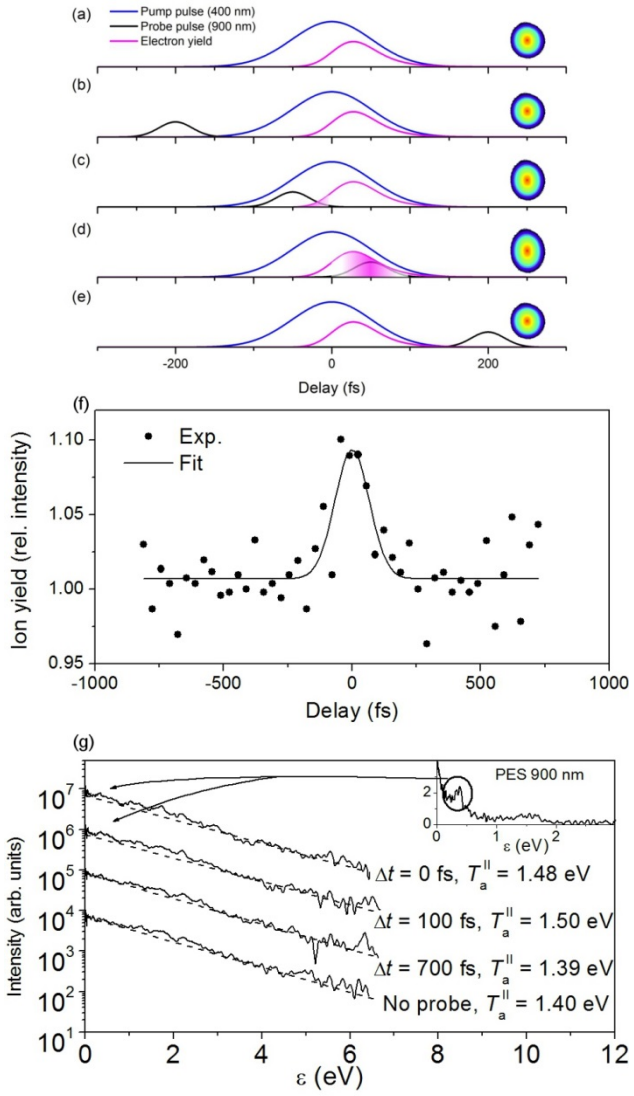

Figure 4. (a – e) Pump-probe scheme. (a) A 400 nm pulse (blue line) is used to create thermal electrons (pink line) resulting in a near-isotropic VMI image (sketch on right-hand side for illustrative purposes (not experimental results)). (b) An IR probe pulse will not cause any asymmetry if the thermal electrons are not emitted during the temporal envelope of the probe pulse. (c – d) When the probe pulse overlaps with the electron yield, the VMI image will become slightly asymmetric. (e) When the probe pulse arrives after the emission of the thermal electrons, the VMI image will not be affected by the pulse. (f) Transient ion yields obtained using a 400 nm, 120 fs, 2 $TWcm^{-2}$ pump and a 900 nm, 60 fs, 5 $TWcm^{-2}$ probe. The transient was fitted to a

Gaussian function giving a FWHM of 160 fs. (g) PES at various pump-probe delays. The spectra have been cut off at the noise level (starting approximately at 6 eV) and shifted vertically for display purposes. Inset shows PES obtained using 900 nm pulses with higher intensity than what was used in the pump-probe experiment (probe alone did not give a signal during the pump-probe experiment). The main 900 nm peak at *ca*. 0.4 eV was also seen in the PES during the pump-probe experiment at delay times close to when the two pulses were temporally overlapped.

In the experiment, the IR field did cause some additional ionization although the amount was small. This is shown in **Figure 4** f), where negative delays correspond to when the IR field leads the 400 nm field. The additional ion signal comes from one-photon ionization by the 900 nm pulse of transiently excited Rydberg-like states and at this particular wavelength, the d "superatom molecular orbital" gives rise to the prominent peak at *ca*. 0.4 eV (see inset in **Figure 4** g).[6,14] This peak was also observed in the transient PES when the two pulses were temporally overlapped (**Figure 4** g). From the same transient angular-resolved PES, the parallel and perpendicular temperatures were recorded and are shown in **Figure 5**. The probe intensity was 5 $TWcm^{-2}$, which corresponds to $U_p = 0.4$ eV. Since the probe pulse is shorter than the expected emission time, only a small fraction of the emitted electrons will be given the extra momentum kick. Therefore, the effect we are looking for is rather weak, and indeed, the asymmetry data are noisy but there is a significant increase in the parallel temperature, starting just before zero time delay and lasting for a few hundred fs. The relatively constant perpendicular temperature indicates that the probe pulse did not cause any significant additional heating and that the increase in parallel temperature is due to the extra push imposed by the probe pulse to the thermally emitted electrons created by the pump pulse. Given the experimental results at hand, delayed electron emission after fs laser excitation seems to take place on a timescale on the order

of 0 – 300 fs after the initial laser pulse, for the conditions used in the experiment. The results are compared to calculated electron yields for the pump laser conditions used (using σ_p = 1.0 Å^2 as in **Figure 3** f). The experimental results indicate a slightly longer emission timescale than the model. However, keeping in mind the simplicity of the model, the agreement is reasonable. The emission timescale is also consistent with the previously estimated vibrational coupling constant of 240 fs[3], the timescale on which the electronic excitation energy is distributed among the vibrational modes, thus cooling the electron gas and reducing the probability for thermal electron emission. This implies a very fast thermalization time for a relatively small particle in the gas-phase but not improbable because of the high initial vibrational temperature at which the molecules are prepared (500 °C). The experimental signal-to-noise ratio could be increased by using an even longer wavelength resulting in a larger effect due to the square wavelength dependence of U_p.

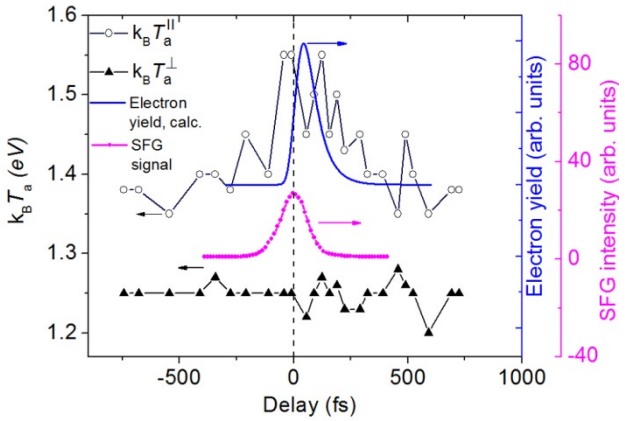

Figure 5. Results from the pump-probe experiments where 120 fs, 400 nm 2 TW cm^{-2} pulses were used to create thermal electrons. The thermal electron distribution was influenced by the 900 nm, 60 fs, 5 TWcm^{-2} probe beam, causing an anisotropy with respect to the parallel and perpendicular apparent temperatures. Due to the relatively high intensity of the 400 nm pulse in this experiment, the parallel temperature was slightly higher than the perpendicular one, even in

the absence of the 900 nm probe pulse. The sum frequency generation (SFG) signal of the two laser pulses is also shown for comparison.

CONCLUSIONS

We have experimentally investigated anisotropic electron emission from C_{60} after fs laser excitation using angular-resolved photoelectron spectroscopy. We found that the observed degree of anisotropy with respect to the exciting laser's polarization direction is consistent with a simple model treating the molecule's valence electrons as a Fermi gas and taking into account the interaction of the emitted electrons with the laser field using classical electrodynamics. The model could qualitatively reproduce the experimental results and therefore give a simple explanation for the observed effects. However, it is clear that several questions remain open since the simple model cannot fully reproduce the measured asymmetry. The presented experimental results should therefore stimulate the efforts of theoreticians working on ultrafast ionization mechanisms of clusters and nanoparticles.

The asymmetry effect was used to measure the timescale for thermal electron emission from C_{60} and it was found that after exciting with 120 fs, 400 nm, 2 TW cm^{-2} pulses, thermal electrons are emitted around 0 – 300 fs after the initial laser pulse. The pump-probe scheme is general and should be applicable to gas-phase clusters and other systems that may show thermal electron emission on a fs timescale. The asymmetric thermal electron distributions shown by several polycyclic aromatic hydrocarbons after fs laser excitation,[13] indicate that the pump-probe scheme could also be used to measure the dynamics of the relatively unexplored phenomenon of thermal electron emission from aromatic organic molecules.

AUTHOR INFORMATION

Corresponding Author

*Eleanor.campbell@ed.ac.uk, Tel: 0044 131 650 4729

Author Contributions

The manuscript was written through contributions of all authors. All authors have given approval to the final version of the manuscript.

ACKNOWLEDGMENT

The authors wish to thank K. Hansen for longstanding collaboration and development of the thermal model. Financial support from the Leverhulme Foundation (RPF-298 "PES of hollow nanomaterials") is gratefully acknowledged.

REFERENCES

1. Johansson, J. O.; Campbell, E. E. B. Probing Excited Electronic States and Ionisation Mechanisms of Fullerenes. *Chem. Soc. Rev.* **2013**, *42*, 5661-5671.

2. Campbell, E. E. B.; Hansen, K.; Hoffmann, K.; Korn, G.; Tchaplyguine, M.; Wittmann, M.; Hertel, I. V From Above Threshold Ionization to Statistical Electron Emission: The Laser Pulse-Duration Dependence of C_{60} Photoelectron Spectra. *Phys. Rev. Lett.* **2000**, *84*, 2128-2131.

3. Hansen, K.; Hoffmann, K.; Campbell, E. E. B. Thermal Electron Emission from the Hot Electronic Subsystem of Vibrationally Cold C_{60}. *J. Chem. Phys.* **2003**, *119*, 2513–2522.

4. Kjellberg, M.; Johansson, J. O.; Jonsson, F.; Bulgakov, A. V; Bordas, C.; Campbell, E. E. B.; Hansen, K. Momentum-Map-Imaging Photoelectron Spectroscopy of Fullerenes with Femtosecond Laser Pulses. *Phys. Rev. A* **2010**, *81*, 23202.

5. Johansson, J. O.; Fedor, J.; Goto, M.; Kjellberg, M.; Stenfalk, J.; Henderson, G. G.; Campbell, E. E. B.; Hansen, K. Anisotropic Hot Electron Emission from Fullerenes. *J. Chem. Phys.* **2012**, *136*, 164301.

6. Mignolet, B.; Johansson, J. O.; Campbell, E. E. B.; Remacle, F. Probing Rapidly-Ionizing Super-Atom Molecular Orbitals in C_{60}□: A Computational and Femtosecond Photoelectron Spectroscopy Study. *ChemPhysChem* **2013**, *14*, 3332-3340.

7. Campbell, E. E. B.; Ulmer, G.; Hertel, I. V Delayed Ionization of C_{60} and C_{70}. *Phys. Rev. Lett.* **1991**, *67*, 1986-1989.

8. Campbell, E. E. B.; Levine, R. D. Delayed Ionization and Fragmentation en Route to Thermionic Emission: Statistics and Dynamics. *Annu. Rev. Phys. Chem.* **2000**, *51*, 65–98.

9. Olof Johansson, J.; Bohl, E.; Henderson, G. G.; Mignolet, B.; Dennis, T. J. S.; Remacle, F.; Campbell, E. E. B. Hot Electron Production and Diffuse Excited States in C_{70}, C_{82}, and $Sc_3N@C_{80}$ Characterized by Angular-Resolved Photoelectron Spectroscopy. *J. Chem. Phys.* **2013**, *139*, 084309.

10. Lassesson, A.; Hansen, K.; Jönsson, M.; Gromov, A.; Campbell, E. E. B.; Boyle, M.; Pop, D.; Schulz, C. P.; Hertel, I. V; Taninaka, A., *et al*. A Femtosecond Laser Study of the Endohedral Fullerenes $Li@C_{60}$ and $La@C_{82}$. *Eur. Phys. J. D At. Mol. Opt. Phys.* **2005**, *34*, 205–209.

11. Schlipper, R.; Kusche, R.; Issendorff, B. V.; Haberland, H. Thermal Emission of Electrons from Highly Excited Sodium Clusters. *Appl. Phys. A Mater. Sci. Process.* **2001**, *72*, 255–259.

12. Maier, M.; Wrigge, G.; Hoffmann, M.; Didier, P.; Issendorff, B. V. Observation of Electron Gas Cooling in Free Sodium Clusters. *Phys. Rev. Lett.* **2006**, *96*, 1–4.

13. Kjellberg, M.; Bulgakov, A. V; Goto, M.; Johansson, J. O.; Hansen, K. Femtosecond Electron Spectroscopy of Coronene, benzo[GHI]perylene, and Anthracene. *J. Chem. Phys.* **2010**, *133*, 074308.

14. Johansson, J. O.; Henderson, G. G.; Remacle, F.; Campbell, E. E. B. Angular-Resolved Photoelectron Spectroscopy of Superatom Orbitals of Fullerenes. *Phys. Rev. Lett.* **2012**, *108*, 173401.

15. Mauritsson, J.; Johnsson, P.; Mansten, E.; Swoboda, M.; Ruchon, T.; L'Huillier, A.; Schafer, K. Coherent Electron Scattering Captured by an Attosecond Quantum Stroboscope. *Phys. Rev. Lett.* **2008**, *100*, 1–4.

16. Bordas, C.; Paulig, F.; Helm, H.; Huestis, D. L. Photoelectron Imaging Spectrometry: Principle and Inversion Method. *Rev. Sci. Instrum.* **1996**, *67*, 2257–2268.

17. Schyja, V.; Lang, T.; Helm, H. Channel Switching in Above-Threshold Ionization of Xenon. *Phys. Rev. A* **1998**, *57*, 3692-3697.

18. Roberts, G. M.; Nixon, J. L.; Lecointre, J.; Wrede, E.; Verlet, J. R. R. Toward. Real-Time Charged-Particle Image Reconstruction Using Polar Onion-Peeling. *Rev. Sci. Instrum.* **2009**, *80*, 53104.

19. Andersen, J. U.; Bonderup, E.; Hansen, K. Thermionic Emission from Clusters. *J. Phys. B At. Mol. Opt. Phys.* **2002**, *35*, R1–R30.

20. Glazer, M.; Wark, *J. Statistical Mechanics: A Survival Guide*, Oxford University Press, 2001

21. Hansen, K. *Statistical Physics of Nanoparticles in the Gas Phase*; Springer, 2013.

22. Mehlig, K.; Hansen, K.; Hedén, M.; Lassesson, A.; Bulgakov, A.V.; Campbell, E.E.B. Energy Distributions in Multiple Photon Absorption Experiments. *J. Chem. Phys.* **2004**, *120*, 4281-4288.

23. Campbell, E. E. B.; Raz, T.; Levine, R. D. Internal Energy Dependence of the Fragmentation Patterns of C_{60} and C_{60}^{+}. *Chem. Phys. Lett.* **1996**, *253*, 261–267.

24. Huismans, Y.; Cormier, E.; Cauchy, C.; Hervieux, P. -a.; Gademann, G.; Gijsbertsen, A.; Ghafur, O.; Johnsson, P.; Logman, P.; Barillot, T.; *et al*. Macro-Atom Versus Many-Electron Effects in Ultrafast Ionization of C_{60}. *Phys. Rev. A* **2013**, *88*, 013201.

25. Bordas, C.; Baguenard, B.; Climen, B.; Lebeault, M. A.; Lépine, F.; Pagliarulo, F. Time-Dependent Spectrum of Thermionic Emission from Hot C_{60}. *Eur. Phys. J. D - At. Mol. Opt. Plasma Phys.* **2005**, *34*, 151–155.

TABLE OF CONTENTS GRAPHIC